Mineralogia, vol. 52, 2021, 19-30 *Original paper*

DOI: 10.2478/mipo-2021-0003

Evidence of amorphous Ca-phosphate precipitate caused by bio mineralisation in 4-5th CE lime plasters of the previously submerged east coastal monument of Salvankuppam

Manager R. Singh[1]*

S. Vinodh Kumar[2]

Kuntikana Ganaraj[3]

[1]National Research Laboratory for Conservation of Cultural Property, E/3, Aliganj, Lucknow 226 024, India
[2]Conservation Research Laboratory, Ajanta Caves, Archaeological Survey of India, Padmapani Bhavan, Dr. BAMU Campus, Aurangabad 431 002, India
[3]Environmental Geotechnology Laboratory, Indian Institute of Technology, Mumbai 400 076, India
*Corresponding author: m_singh_asi@yahoo.com

Abstract

The lime plasters of the excavated monument of Salvankuppam, previously submerged and exposed by the Tsunami occurred in the Indian Ocean on 26th December 2004 was studied with different analytical techniques. The temple is dated 4-5th century CE. The XRF, XRD, FTIR, NMR, SEM-EDX analysis of the lime plasters evidenced particular occurrence of phosphatised bacterial remains in saline conditions. The formation of amorphous Ca-phosphate by bio mineralization was identified in the plasters by the analyses. The plasters are made of air-lime with coarse aggregates and seashells inclusion as confirmed by the thermal and chemical analysis. The microstructure and morphological investigations of mineralized microbial structures by SEM-EDX indicated the formation of amorphous Ca-phosphate. The unordered and fibrous spherulites have hardened and reduced porosity of the plaster by bio mineralization as observed through MIP analysis. The 16S rRNA sequencing has identified the Pseudomonas strains mainly responsible for the clustering of amorphous Ca-phosphate particles around the bacterial colony.

Keywords: Amorphous Ca-phosphate, lime plasters, 16S rRNA, Bio-mineralization, calcite

1. Introduction

The damage to historical plasters and mortars worldwide is occurring mainly due to the ingress of water and environmental parameters (Amoroso et al. 1983; Camuffo 1995; Pedro, Jorge 2008;). Any intrusion of contaminated or saline water into the ancient plasterworks causes greater damage due to the presence of dissolved salts and minerals. The lime plasters exposed to saline conditions in coastal regions show intense damage. Moreover, the plasters and mortars used in historical structure submerged in the sea in the past behave differently on exposure to the coastal environment. An example is South India's east coast monument of Salvankuppam which is 6 km north of 7th century AD shore temple, Mamallapuram, a World Heritage Site. On 26th

December 2004 Tsunami in the Indian Ocean exposed a 10th-century inscription engraved on a rock boulder. Subsequently, an excavation was undertaken by the Archaeological Survey of India leading to the discovery of an ancient Hindu temple. Based on the archaeological evidence and different phases of building activity the temple was dated from 4-5th BCE to 12-13th BCE (Satyabhama et al. 2011). The main building blocks used in construction are the manmade brick foundation, laterite stone blocks, and granite slabs cemented together by lime mortar as binder and lime plastered.

On exposure to saline winds of east coast Indian Ocean and sunlight, the mortars and plasters of exposed monument started getting weaker with the evaporation of water on drying. This caused weakening and detachment of the plaster layers besides the powdering of constituent materials with time. The mineralogical and micro-structural compositions of the plasters were studied to safeguard the historical, aesthetic, and cultural values of the site.

The literature survey for the stabilization of plasters and mortars recommends water repellent in the form of chemical reinforcement (Sigel et al. 2008). However, owing to the irreversible nature of the repellent coating and saline condition, the chemical methods have not proved effective for coastal lime works in the long run (Camaiti et al. 1988; Lowenstam, Weiner 1989; Franzoni et al. 2015). Therefore, to preserve the soft and friable plasters in highly unfavourable saline conditions without any chemical reinforcement, researchers developed the biomineralization technique (Castanier et al. 1984; May 2001). The main aim of this method was to create a biofilm on the plaster/mortar surface to act as a protective layer against environmental factors to limit or avoid damage to historical structures (Rodriguez-Navarro et al. 2003).

The biologically controlled mineralization alters the structural features of lime plasters by the formation of amorphous Ca-phosphate precipitation in saline conditions. The combination of microbial metabolic waste and the surrounding environment have taken part in the formation of biominerals in the plaster (Jawaid et al. 2018). It has been reported that nucleation of amorphous Ca-phosphate (ACP) in a transient state in the precipitation of aragonite by halophilic bacteria and physicochemical conditions of the culture medium play a vital role in Ca-phosphate precipitation (Ravadeneyra et al. 2010). A previous study has reported that the dried ACP can exist in discoidal and spheroidal forms (Eanes et al. 1973). It has been demonstrated that pseudomonas strains can precipitate calcium and amorphous calcium phosphate on the surface of their strains (Fishman et al. 2018). The biomineralization of lime plasters occurs with the induction of biosystems. The lime plasters of the Salvankuppam temple also showed the microbial intervention that will be studied in detail in this paper.

In the present work, we envisage the role of bacteria in the formation of ACP within the lime plaster of the Saluvankuppam temple in saline conditions. Therefore, the instrumental techniques of X-ray diffraction studies (XRD), X-ray Fluorescence Spectroscopy (XRF), Scanning Electron Microscope – Energy Dispersive X-ray analysis (SEM-EDX), particle size analyzer, Fourier Transform Infrared Spectroscopy (FTIR), Nuclear Magnetic Resonance Spectroscopy (NMR) and thermal analysis were used to characterize the mineralogical and chemical composition of the plasters. The mercury intrusion porosimetry (MIP) was used to measure porosity and pore size distribution of the plasters. The microbial population was cultured in the laboratory and 16S rRNA sequencing was used in the identification of bacterial strains.

2. Sampling and Location

Figure 1a shows the General view of the site and Figure 1b shows the location map of the temple. Based on the architectural and epigraphic evidence, the temple is dated to the Pallava period and constructed from 4-5th BCE to 12-13th BCE with many phases of building activity (Rajendran et al. 2006). The radiocarbon dating of charcoal pieces from the temple reported a period of 405-1091 AD (Sundaresh et al. 2004). An alternative report mentions the occurrence of long-term sea-level rise and severe coastal erosion as the main causes for submergence and destruction of the temple (Sundaresh et al. 2004). The exposed laterite and manmade bricks were plastered with a fine lime probably prepared at the site since lime kilns, seashells, and saddle querns were found at the site during excavation (Rajendran et al. 2006).

Salavankuppam is located very nearer to Mahabalipuram that has a tropical wet-dry climate which comes under the Koppen – Geiger climate classification. That means that the winter, receives less rainfall than in the summer (Kumar, Singh 2019). As per the temperature, Relative Humidity and Rainfall recorded in the automatic weather station (AWS) installed in the Shore temple complex, Mahabalipuram the maximum temperature recorded for a year is in the range of 29°C to 40°C and the minimum temperature is in the range of 18°C to 23°C. The relative humidity recorded varies in between 31% to 98.97% during different seasons. In one year the average rainfall is 1219 mm. In high relative humidity (RH more than 50%) conditions, the formation of aerosols with the salt particles occurred in marine environment and deteriorates the plasters of the temple. The hot, humid and salty environmental parameters are the conservation threat to the excavated temple.

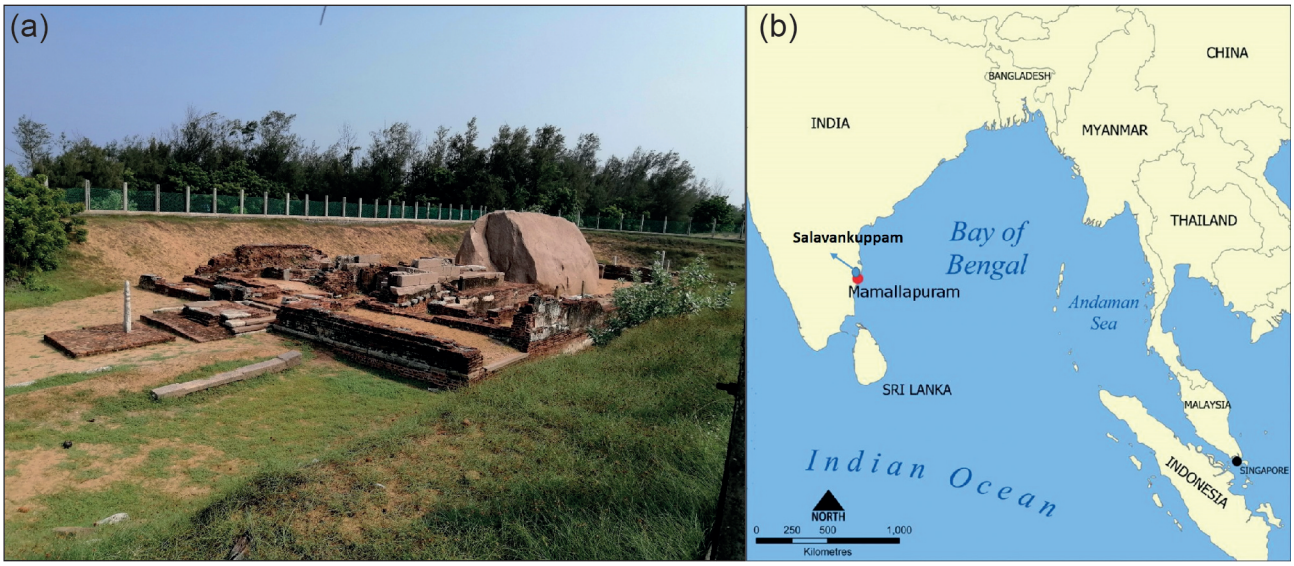

Figure 1. (a) General view of excavated temple complex of Salvankuppam. (b) Location map of Salavankuppam temple.

3. Materials and Methods

Six numbers of lime plaster samples (S1-S6) were extracted from the excavated temple complex. Plaster samples S1, S5, and S6 were extracted from eastern, western, and northern walls cloister mandapa and the samples S2, S3, and S4 represent eastern, southern, and western walls Mukhamandapa of the temple, respectively. Figure 2a-d shows the lime plasters and the sample collection locations. All the samples were washed with ethanol by rinsing to remove any contaminants before carrying out various instrumental analyses.

All the plaster samples were analyzed by X- ray diffraction (model Philips Pan Analytical Xpert) for the identification of minerals. The samples were finely grinded and analyzed under a CuKα radiation source in a 2θ range of 5-90° at 45 kV. The diffractograms were analysed using Xpert High score software for its mineralogical contents. Samples (S1-S6) were analysed by X- Ray Florescence Spectroscopy (Model Artax 200, Bruker, Germany) at a voltage of 50 kV at 700 mA current, and data collection time was 300 life seconds. At least 4 measurements were performed for each sample and data averaged. The chemical compositions are reported in oxide form

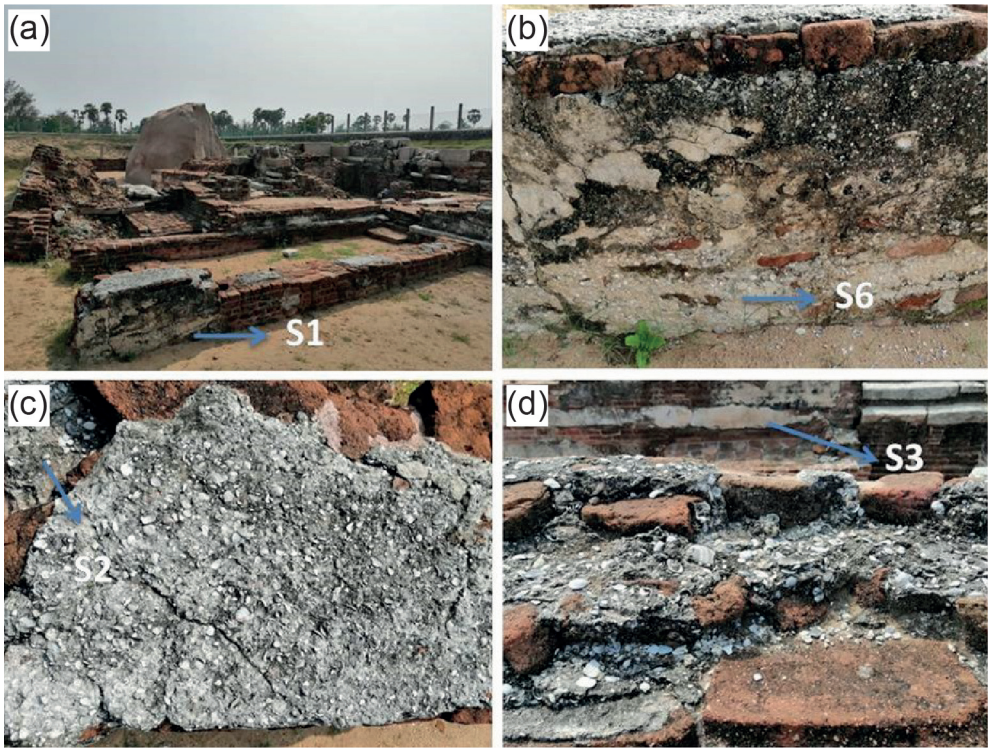

Figure 2. (a) General view of excavated temple complex of Salvankuppam; (b) lime plaster of the temple; (c) lime plaster of the temple with sea shells; (d) lime plaster of the temple with sea shells (sample collection locations mentioned with arrows).

of the elements. The morphology of all the samples was captured with an FEI Quanta 200 scanning electron microscope. The backscattered electron images (BMI) and secondary electron images (SCI) were recorded at a high vacuum coupled to an energy dispersive X-ray (EDS) analysis at an accelerating voltage of 20 kV. The elemental compositions were obtained through the software available with the system using a standard technique and matrix correction. SEM-EDX elemental mapping for phosphorus was also performed for the plaster samples. The pore size distribution (PSD) of all samples was determined with the help of mercury intrusion porosimeter (MIP) employing pore master 60 (Quantachrome, USA). The mercury is a non-wetting fluid, has a greater contact-angle ($\Theta = 140^{o}$) and surface tension (σ = 0.48 N/m) values. Its intrusion into the pores would be possible only by the application of external pressure. The cumulative volume of the mercury intruded into the sample was recorded with the help of pore master software. The pore size distribution was obtained from the cumulative volume of the mercury (Vm) intruded at any pressure. The specific gravity, G of the samples was measured using an ultra-pycnometer purging the helium gas. Before particle size analysis, all the salt marks and organic materials from the samples were removed with alcohol. The laser particle size analyzer was used to find the proportions of clay, silt, and sand-size particles in the samples. Plaster samples S1 to S6 were used for particle size analysis. The particle size analysis of lime plaster of Subbramanya temple, Salavankuppam provided the size distribution curve through which the aggregates of the plasters were characterized. The percentages of gravel, sand, silt and clay size particles present in the aggregate were derived from the particle size distribution curve. The FTIR analysis of samples (S1-S6) was performed with a 3000 Hyperion Microscope with Vertex 80 FTIR system (make Bruker, Germany) with a focal plane array: 128x128, scanning wavelength range between 4000-400 cm^{-1}. The KBr pellet technique was used and the spectra were recorded at 4 cm^{-1} resolution and the number of scans was 32 within the standard wave number. The precision of the instrument was ± 5 cm^{-1}.

^{31}PNMR analysis of samples S2 and S6 has been performed with ECZR series 600 MHz NMR spectrometer (Jeol, Japan) to understand the phosphate deposition. The solid-state Cross polarization- Magnetic Angle Spinning CP/MAS probe with 3.2 mm rotor having a fast magic angle spinning at 20 kHz speed that covers nuclei in the range of 15N to 31P was used. The spectrum was processed with the Delta NMR data processing software. The sequential thermal analysis of all the samples was performed with the help of STA 8000 (Perkin Elmer) in a nitrogen environment. The gas pressure was maintained at 2 bar and the flow rate has been regulated to 30 ml/min. The thermal stability of the samples was determined by the weight loss occurring in the sample.

Samples S1 and S4 were selected for microbial identification. 1.0 gm of the sample was introduced into a sterile conical flask containing 100 ml peptone water, incubated at 37˚C for an hour, and subjected for plating on nutrient agar plates. The isolate was isolated, cultured, and further preserved on Luria agar slants for use. The genomic DNA of the isolate was extracted and purified by Anyprep Bacterial Genomic DNA Miniprep kit as per the manual and its purity and quantification accomplished by nanodrop (Thermo, USA). Universal 16S rRNA PCR forward and reverse primers were used in the amplification of 16S rRNA genes. The PCR reaction was analyzed by 1.2% agarose gel electrophoresis, amplified product in the gel was cut by clean scalpel, purified by Quigen quick PCR purification kit and DNA was sequenced by Xcleris, India. The obtained 16S rRNA sequences were further subjected to the BLAST program (http://www.ncbi.nlm.nih.gov/) to confirm the organisms.

4. Results

4.1. XRD Analysis

The major crystalline phases identified in the samples through X-ray diffractogram are calcite, quartz, and orthoclase ($KAlSi_3O_8$) as shown in Fig. 3 for all the plaster samples. The presence of minerals calcite, quartz, and aluminosilicates was confirmed by JCPDS (Joint Committee on Powder Diffraction Standards) data. The presence of calcite and aragonite may be attributed to the addition of sea shell aggregates in the preparation of the plaster which can be seen by the naked eyes. During excavation, the sea shells storage within the temple complex was found along with ancient lime kilns (Satyabhama et al. 2011). The presence of aragonite, polymorph form of $CaCO_3$ was also confirmed with the XRD spectra.

4.2. XRF Analysis

The Salvankuppam lime plasters are rich in calcium oxide as it makes more than half part of the plaster. The calcium oxide percentage (Table 1) was found varying between 42.66 to 63.01 wt% in the plaster. The next major element is silica as SiO_2 percentage in the plaster varies between 19.02 to 36.06 wt%. Iron oxide is present in major quantity and its content varies between 3.71 to 10.80 wt% in the plaster. The wt% of alumina in the plaster samples is always low and varies between 1.54 to 2.34 wt%. The K_2O and TiO_2 are present in minor quantities in all the samples. Interestingly, in all the samples presence of phosphorus was observed and its content varied between 1.54 to 2.34 wt%.

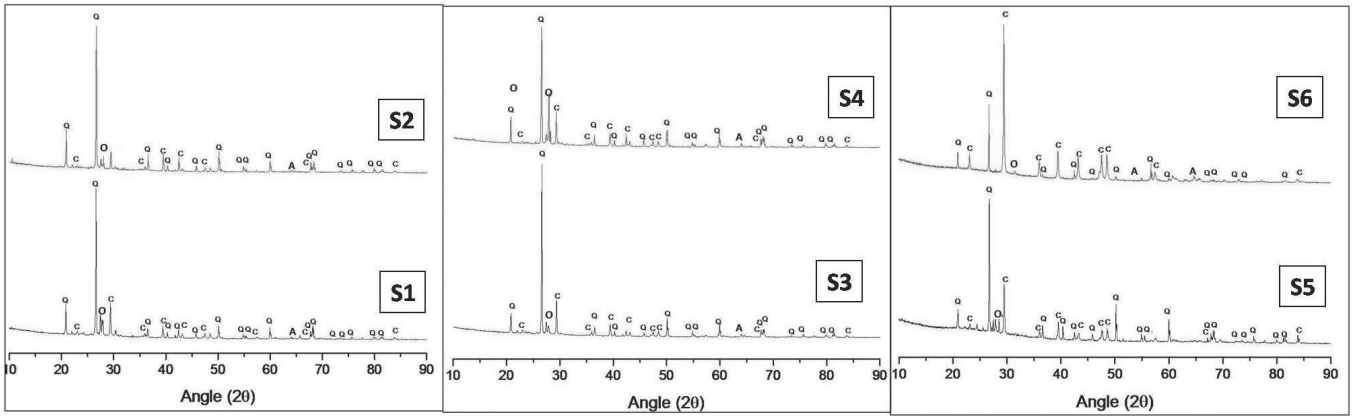

Figure 3. XRD Spectra of lime plaster samples of Salvankuppam (Cal – calcite; Arg – Aragonite; Qz – quartz; Or – orthoclase).

4.3. SEM-EDX Analysis

The amorphous calcium phosphate precipitated by bacterial strains was observed using Scanning Electron Microscope at different magnification. The SEM images of samples S2, S3 and S6 are shown in Fig. 4. The plasters have a compact structure with aggregates well embedded in the matrix. Figure 4a-f shows that all the bright particles on the surface of solid substrate of the plaster are mineral fragments, with angular crystalline morphology. The white halo amorphous Ca-phosphate formed around the bacterial colony is looking unordered and fibrous at high magnification (Fig. 5). The dried amorphous Ca-phosphate exhibits spheroidal morphology. The microstructure of these spherulites showed that they are aggregates of well defined elongated platy crystals. EDS analysis of the sample has been performed on the outer and the inner layer of the samples to obtain the chemical composition. The same has been shown in Figure 6. From the elemental composition (EDX) analysis for plaster samples S1 to S6, it is observed that all the plasters contain the range of Phosphorous from 0.59 to 4.21wt%.

4.4. Porosity and Pore size distribution

The porosity and pore structures are linked to grain size and binder/aggregate arrangement within the plaster matrix. For typical lime plasters, the size and distribution of pores are associated with aggregate grains, carbonation rate, and distribution of carbonate crystals. Within the pores there may be secondary fine-grained calcite or salt crystallization. The porosity in the plaster mainly develops during its hardening phase (Papayianni, Stefanidou 2001) and any organic materials containing protein if added give rise to round-shaped voids (Sickels 1982).

As the plaster is made up of heterogeneous materials, the complexity of the pore structure makes the interpretation of porosity rather difficult. Moreover, the pore size distribution, the total porosity, and specific surface area are also used to assess the mechanical properties of the plaster. The porosity of the sample is shown in Tables 2 and 3 along with specific gravity (G) values for the plasters. The pore size distribution and differential pore volume depicting the dominant pore diameter for plaster samples S1-S6 is shown in Fig. 7. As the physical

Table 1. Chemical composition (weight %) of the lime plaster samples, Salvankkuppam.

Sample No	SiO_2	Al_2O_3	Fe_2O_3	CaO	MnO	Na_2O	K_2O	TiO_2	P_2O_5	Total
1	36.06 ±1.62	2.2 ±0.46	8.51 ±0.81	42.66 ±1.82	-	1.15 ±0.05	6.31 ±0.50	1.05 ±0.06	1.79 ±0.07	99.73
2	27.7 ±1.43	1.4 ±0.36	3.71 ±0.90	58.02 ±1.91	-	1.25 ±0.05	2.46 ±0.30	4.09 ±0.35	2.01 ±0.08	100.64
3	26.87 ±1.44	3.26 ±0.50	1.1 ±0.45	61.68 ±1.55	0.39 ±0.02	0.36 ±0.03	2.31 ±0.05	1.65 ±0.46	1.54 ±0.02	99.16
4	29.5 ±1.25	1.25 ±0.44	5.73 ±0.67	56.73 ±1.95	1.43 ±0.04	0.22 ±0.05	1.05 ±0.46	1.15 ±0.56	2.35 ±0.09	99.41
5	26.99 ±1.42	1.75 ±0.35	7.66 ±0.77	55.67 ±1.68	0.98 ±0.05	0.65 ±0.06	2.12 ±0.50	2.29 ±0.50	1.45 ±0.07	99.56
6	19.02 ±0.98	0.79 ±0.41	10.8 ±0.57	63.01 ±1.62	0.23 ±0.03	0.49 ±0.50	1.63 ±0.42	1.05 ±0.50	2.15 ±0.09	99.17

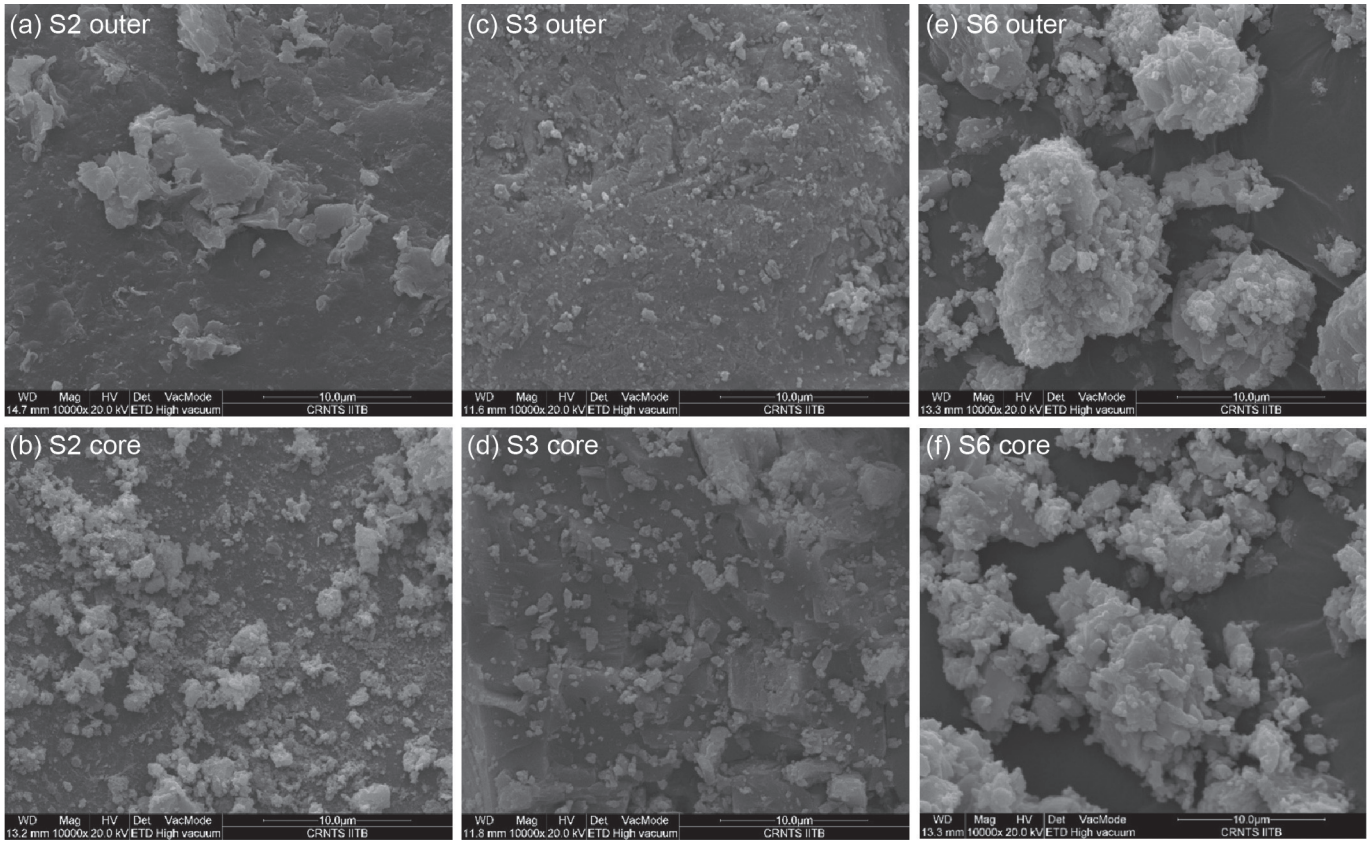

Figure 4. SEM images of lime plasters, Salvankuppam; samples S2, S3 and S6.

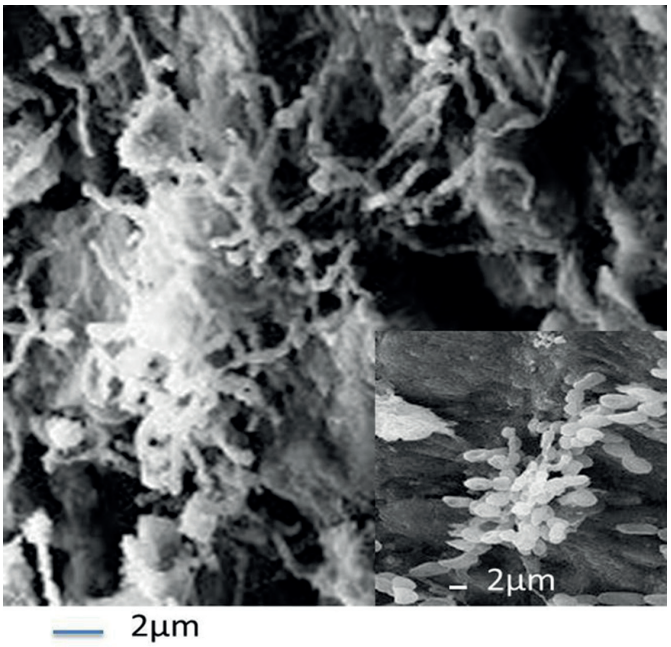

Figure 5. SEM images of bacterial colony found along with white halo amorphous Ca-phosphate in lime plasters of Salvankuppam.

appearance of the outer and core layer of the lime plasters was different, the determination of porosity of outer layer and the porosity of core layer was carried out.

The porosity percentage (n = 6.21-19.14%) obtained through MIP clearly shows that most of the plasters have an average porosity of 14-15% except Sample S4 (8.86%) and S5 (6.21%). From Fig. 7a and 7b, it is seen that the

Table 2. Porosity Levels of Core and outer layers of the samples.

Sample No	Sample ID	n	macro	meso	micro	d_d
			(%)			(µm)
1	S2 Core	19.13	89.91	6.57	3.52	122 0.16
2	S2 Outer	15.71	99.76	0.23	0	25.1
3	S3 Core	17.4	100	0	0	67.65
4	S3 Outer	21.7	100	0	0	25
5	S6 Core	14.39	100	0	0	65.76 1.68
6	S6 Outer	12.21	100	0	0	57.22

Table 3. Porosity of the samples determined through MIP analysis.

Sample No	Sample ID	Porosity (n %)	Specific Gravity (G)
1	S1	14.38	2.86
2	S2	19.14	2.86
3	S3	17.41	2.83
4	S4	8.86	2.97
5	S5	6.21	2.8
6	S6	12.94	2.85

outer and core of the samples S3 and S6 have the presence of 100% macropores. Interestingly, in the sample S2, the percentage of macropores is more at the surface

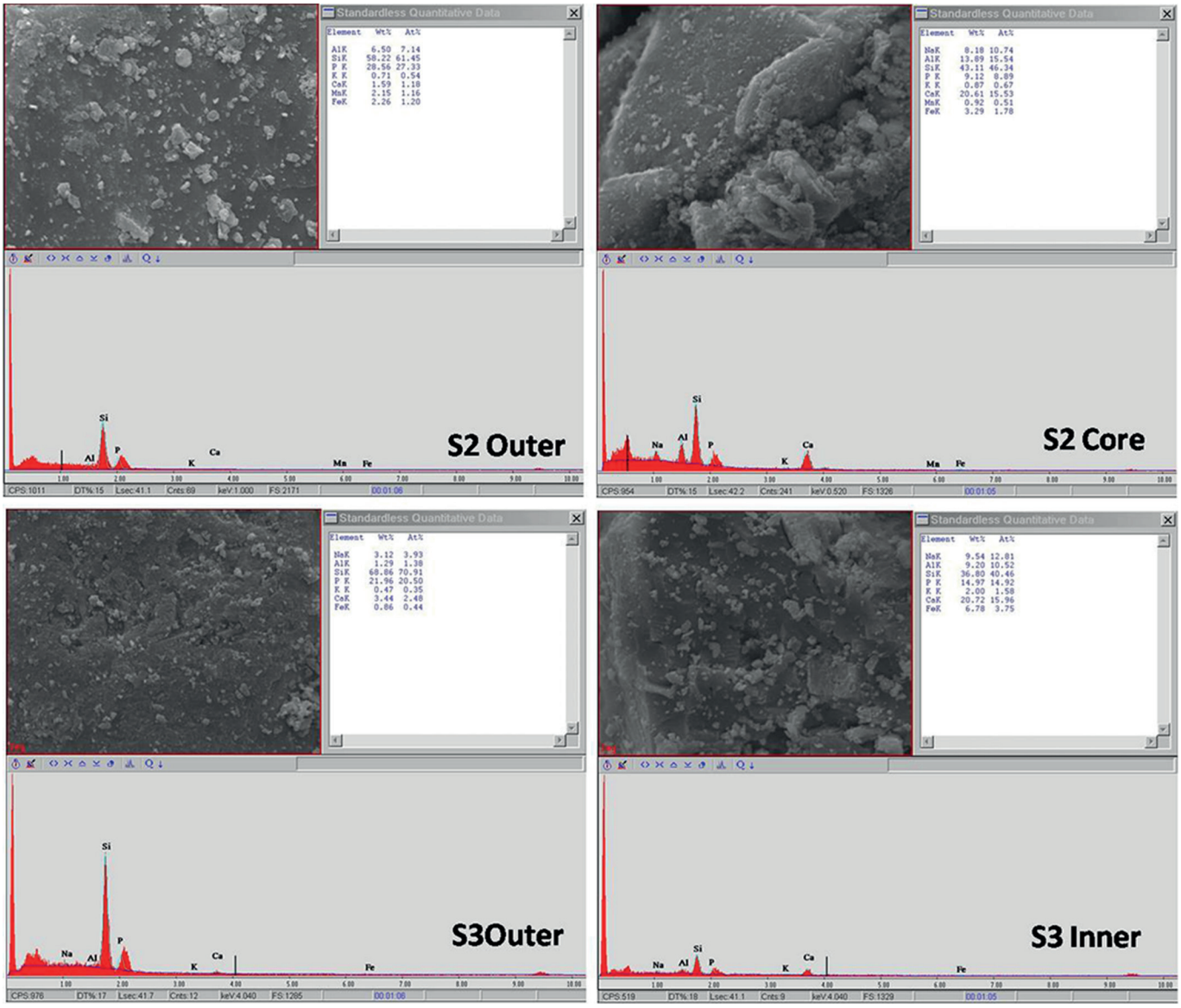

Figure 6. SEM images with EDX spectra of lime plasters of Salvankuppam; samples S2 and S3.

Table 4. Proportions (wt%) of grains of various size present in lime plaster.

Sample No	Grain Type	Sample S1	Sample S2	Sample S3	Sample S4	Sample S5	Sample S6
1	Granule	7	-	8	4	3	12
2	Very coarse sand	8	8	7	10	5	-
3	Very coarse sand	5	7	5	8	9	4
4	Medium sand	10	10	9	7	13	8
5	Fine sand	27	30	27	30	31	32
6	Silt	38	35	36	34	33	35
7	Clay	5	10	8	7	6	9

layer that of the core. It is also observed that the percentage of mesopores and micropores is very negligible in all the samples as compared to its macropores. This reflects an increase in the capillary porosity of the plasters.

4.5. Particle size Analysis

From the particle size analysis, it is observed that the lime plaster aggregates is less fine and contains more silt size particles. The Proportions (wt%) of grains of various sizes present in lime plaster is shown in Table 4. The grain size analysis showed the majority of grains are of silt particles (more than 55%), followed by fine sand particles (35-40%) and least the clay particles (5-10%). A well graded soil will have a uniformity coefficient greater than about 4 for gravels and 6 for sands, and 3 coefficient of gradation between 1 and 3 (for gravels and sand). A soil might have a combination of two are

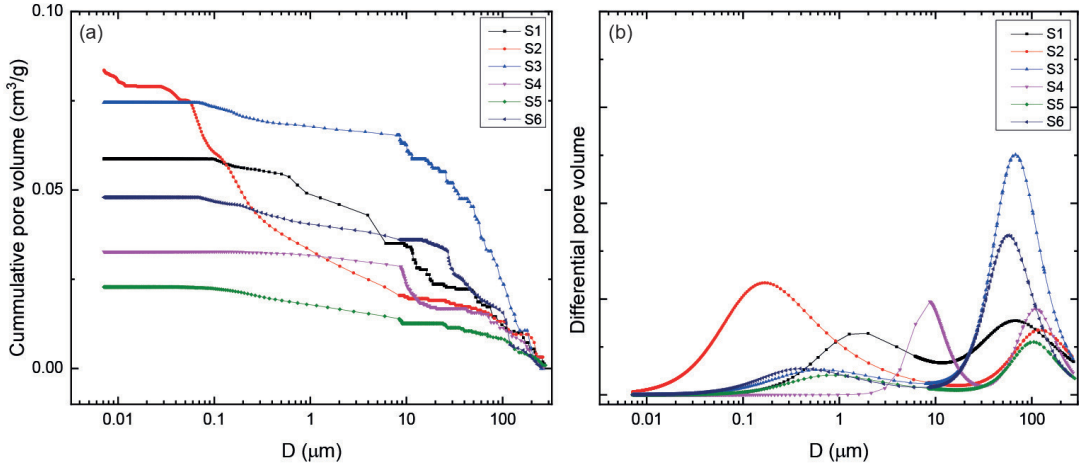

Figure 7. The results of MIP analysis for different samples with (a) cumulative pore size distribution curves, (b) differential pore volume depicting the dominant pore diameter.

more uniformly graded fractions. From the particle size distribution curve, it is found that the aggregate that has been used for the preparation of plaster is well graded. It is clear that the lime plaster milling might have been done before using the lime plaster for construction due to presence of more proportion of silt and sand size particles.

4.6. FTIR Analysis

The FTIR vibrational peaks of all the samples are shown in Fig. 8. Figure 9 shows the inset FT-IR Spectra. The peaks around 2950 cm^{-1} and 2870 cm^{-1} may be due to the C-H stretching of the aliphatic group denoting the presence of protein from the bacteria (Gadd et al. 2003; Tao 2013). The C-H stretching peaks may also be due to the oxidation of proteinaceous additives in the plaster. There is a traditional practice in India to mix adhesive extract of plants for strength, durability (Ravi et al. 2018) and to enhance the waterproof properties of the plaster (Nogueira et al. 2018). The addition of protein also acts as an air-entraining agent and increase the workability of the plaster (Zhao et al. 2015; Elert et al. 2019).

The broad peak around 3500 cm^{-1} may be attributed to hydroxyl group due to the presence of moisture content in the plaster. The main vibrational peaks of phosphate groups are (i) 1086 and 1022 cm^{-1} (PO_4^{3-} v_3) along with a broad peak of quartz around 1000 cm^{-1} (ii) 962 cm^{-1} (PO_4^{3-} v_1) (iii) 600 cm^{-1} (PO_4^{3-} v_4) and 570 cm^{-1} (PO_4^{3-} v_2) (Raynaud et al. 2002; Han et al., 2006; Mabasherpour et al. 2007; Destainville et al. 2003; Eisa et al. 2015). The presence of felspar has also been noticed. The presence of a strong band centered around 1425.4 cm^{-1} is characteristic of the C-O stretching mode of carbonate (CO_3^{2-}) together with a narrow band around 875.68 cm^{-1} of the bending mode (CO_3^{2-} v_2) (Kanth, Singh 2019; Singh, Vinodh Kumar 2019). The peaks near 1800 cm^{-1} and 2515 cm^{-1} represent calcite of the plaster. The peak near 1560 cm^{-1} may be assigned to C=O stretching v_1 of the amide group indicating the presence of microbes in the plaster.

4.7. NMR Analysis

The lime plaster samples S2 and S6 were analyzed under ^{31}P NMR. The NMR shift is shown in Fig. 10. The shift observed in sample S2 is 3.879 and in sample S6 is 4.125. Since the chemical shift is in the range of 0-10 ppm, the

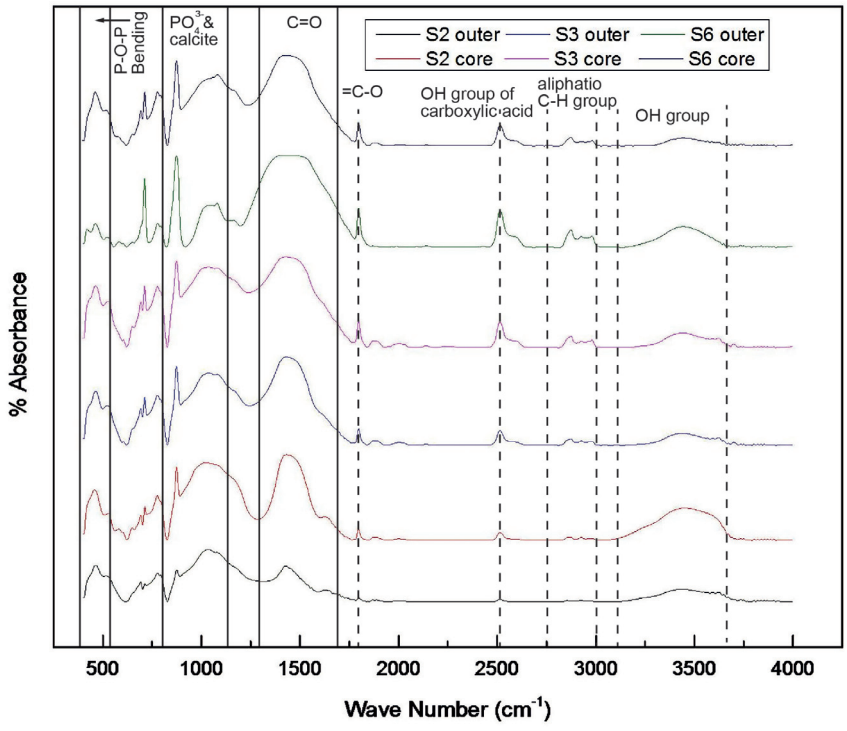

Figure 8. FTIR spectra of the lime plaster samples; samples S2, S3 and S6.

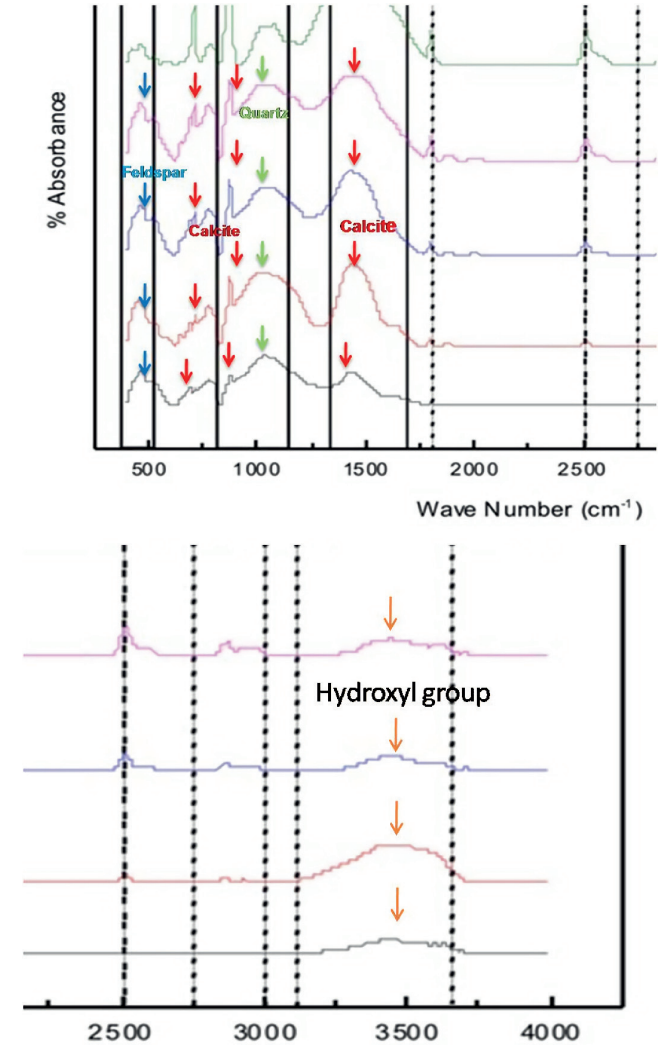

Figure 9. Inset FTIR spectra of the lime plaster samples.

possible compounds in the plaster may be phosphate monoester or orthophosphate (Atkins 1923). The presence of phosphate is confirmed with NMR results. There is the possibility of formation of amorphous Ca-phosphate.

4.8. Thermogravimetric and Differential Thermal (TG-DTA) analysis

The thermal stability of the plaster samples was determined by weight loss occurring in the samples. As observed from TG-DTA curves (Figure 11), the weight loss between 200°C to 600°C mainly due to structurally bound water of clay is very less for all the plasters. The major weight loss observed is in the range of 600-825°C which could be due to the presence of $CaCO_3$ also supported through XRD analysis. Among the samples analyzed, S6 showed a greater percentage of weight loss (≈ 30%) as compared to other samples where weight loss is in the range of 10-13%. The weight loss may be attributed to the presence of non-hydraulic air lime in the plaster samples. Such lime plasters can retain much water against the absorption of masonry units. Moreover, a shift in the DTG curve is also noticed at a temperature between 700-800°C (Figure 11a). The heat flow in the samples was plotted against temperature (Figure 11b) and a small curve was observed at around 600°C for the samples beside a deep curve at around 800°C.

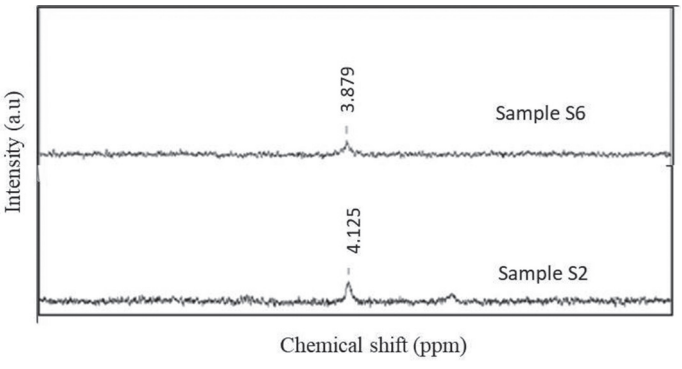

Figure 10. NMR Spectra of lime plaster samples S2 and S6 of Salvankuppam.

4.9. Identification of bacterial isolates

The bacterial culture showed specific types of bacterial cells that survived in the sample and mainly responsible for bio-mineralization. The presence of live bacteria also implies environmental conditions responsible for the viability of bacterial cells. Proper identification of the bacterial isolates is an essential task in microbiology. A total of three microbial strains were isolated from the carbonate-rich plaster. The isolated three potential organisms were identified by 16S rRNA gene sequencing. The 16S rRNA region was amplified as a single amplicon with a 16S primer set. The homology of the 16S rRNA sequence was matched to the NCBI library database. Depending on the percentage of matches and total mismatches, the strains were identified as 1. Bacillus amyloliquofaciens 2. Uncultured Pseudomonadaceae bacterium 3. Pseudomonas stutzeri. A SEM image of bacterial colony found in lime plasters of Salvankuppam is shown in Fig. 5.

5. Discussion

From the porosity and pore size distribution studies, it is observed that all the samples show an identical trend except sample S2 which may be due to the presence of more clay in sample. This increase in capillary porosity of lime plasters is linked to the variation of the evaporation rate of the water from the plaster surface. The variation in the evaporation rate of the water is also due to working conditions, ambient, and rate of the application of wet plaster. This impacted the drying rate of the wet plaster on the surface and its inner core. The irregularity in the surface morphology of the plasters is also due to induced variation of evaporation on the surface and inner core on account of ambient conditions. The porosity of the samples correlates with the particle size analysis of the plasters.

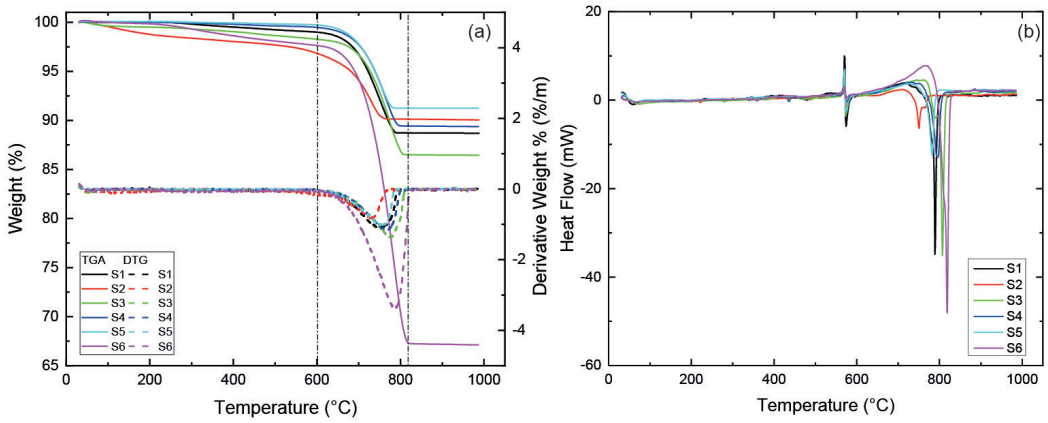

Figure 11. (a) The TG-DTA analysis of the samples. (b) The heat flow curve during sequential thermal analysis; samples S1 – S6.

The FTIR peaks around 2950 cm^{-1} and 2870 cm^{-1} may be due to the C-H stretching of the aliphatic group denoting the presence of protein from the bacteria. The main vibrational peaks of phosphate, calcite, quartz and orthoclase were identified from the FTIR spectrum. NMR spectrum confirmed the presence of phosphate in the plaster. The major minerals identified in the samples through X-ray diffractogram are calcite, quartz, and orthoclase. As the morphology of amorphous Ca-phosphate was unordered and fibrous, it could not be detected through the XRD analysis of the plaster.

XRF results showed that the major components of the plasters are CaO and silica with K_2O, P_2O_5 and TiO_2. This finding is further supported by EDX analysis and phosphorus mapping of the plaster. SEM- EDX results showed that amorphous Ca-phosphate particles have clustered around the bacterial colony and vary in size, shape, and number depending on the Pseudomonas strains. The dried amorphous ca-phosphate exhibits spheroidal morphology.

Pseudomonas bacteria live in a diverse environment (Rainbey 1999; Molina et al. 2000) and have the ability to precipitate calcium (Fishman et al. 2018). In phosphate sequestering pseudomonas species, the precipitation of calcium results in apatite formation (Hammes et al. 2003; Connolly et al. 2013). Many pseudomonas species precipitate amorphous Ca-phosphate (Fishman et al. 2018). It has been reported that some pseudomonas species form brown or white halo amorphous Ca-phosphate on the agar adjacent to the bacterial colony (Turner et al. 2017). The amorphous Ca-phosphate is non-structures and has different morphology. The dried amorphous Ca-phosphate can exist in discoidal and specoidal forms (Eanes et al. 1973). The 16S rRNA sequencing of bacterial strains showed the presence of uncultured pseudomonal bacteria in the plaster. Probably, the bacterial population precipitated amorphous Ca-phosphate through the process of biomineralization (Cosmidis et al. 2015).

The carbonate-based plaster materials contain a variety of habitats constituted by the great diversity of organisms performing a variety of functions. The major category of microbes, bacteria propagate quickly and exist in large quantities in many extreme environments that were previously believed to be unfavorable for life. Bacteria, along with other microorganisms are essential components of our ecosystem and play a key role in material and energy cycling. In the present investigations the microbial isolates from plaster materials may have a role directly or indirectly in calcium and phosphate mineralization. These results are in line with the finding reported in previous studies (Mpanga et al. 2018). Mpanga et al. (2019) investigated the application of Bacillus amyloliguefaciens towards phosphate mineralization and showed its active role in the enhancement of phosphate solubilization. Li et.al. (2012) studied the dynamics of calcium carbonate ($CaCO_3$) precipitation induced by microbial intracellular and extracellular enzymes over a different range of pH. The biogenic apatite has applications in the medical and conservation field and could be used for preservation purposes (Koutsopoulos 2002).

6. Conclusion

The study of ancient lime plasters of temple which was submerged in the sea near Mahabalipuram yielded the presence of phosphatised bacterial remains in the plaster. The porosity percentage (n = 6.21-19.14%) obtained through MIP clearly showed that most of the plasters have an average porosity of 14-15% probably due to the hardening of the plaster by biomineralization or deposition of salts within the pores. The porosity of the samples correlates with the particle size analysis of the plasters. From the granualometric analysis it is found that the aggregate that has been used for the preparation of plaster is well graded. Calcite and silica are the major components that are found from the XRF analysis. SEM images confirm the presence of amorphous Ca-phos-

phate particles clustered around the bacterial colony and vary in size, shape, and number depending on the Pseudomonas strains. The existence of the lime plasters of the temple in this type of microclimatic conditions demonstrates the quality of ancient India lime plaster technology.

Acknowledgements

The authors express their gratitude to the Archaeological Survey of India for the support. We are especially thankful to Prof. D.N. Singh, Indian Institute of Technology, Mumbai and Sh. Ghanshyam, NRLC Lucknow for extending help in the analysis of the samples. We are thankful to M/s Bioraj Laboratories, Nagpur for the bacterial sequencing of microbes.

Conflicts of interest

The authors have no conflicts of interests to declare.

References

Amoroso, G.G., Fassina, V., Lewin, SZ. (1983). *Stone decay and conservation: atmospheric pollution, cleaning, consolidation and protection.* Amsterdam: Elsevier.

Atkins, W.R.G. (1923). The Phosphate Content of Fresh and Salt Waters in its Relationship to the growth of the Algal Plankton. *Journal of the Marine Biological Association of the United Kingdom, 13*(1), 119–150.

Camaiti, M., Borselli, G., and Matteoli, U. (1988). Prodotti consalidanti impiegati nelle operazioni di restauro. *Edilizia, 10*(2), 438 – 445.

Camuffo, D. (1995). Physical weathering of stones. *Science of the Total Environment, 167*, 1-14. DOI: 10.1016/0048-9697(95)04565-I

Castanier, S., Maurin, A., & Bianchi, A. (1984). Participation bactérienne *à* la production du carbonate. *Comptes Rendus de l'Académie des Sciences, 299*(19), 1333–1336.

Connolly, J., Kaufman, M., Rothman, A., et al. (2013). Construction of two ureolytic model organisms for the study of microbially induced calcium carbonate precipitation. *Journal of Microbiological Methods*, *94*(3), 290-299. DOI: 10.1016/j.mimet.2013.06.028

Cosmidis, J., Benzerara, K., Guyot, F., Skouri-Panet, F., Duprat E., Férard C., Guigner J.-M., Babonneau F., & Coelho C. (2015). Calcium-Phosphate Biomineralization Induced by Alkaline Phosphatase Activity in Escherichia coli: Localization, Kinetics, and Potential Signatures in the Fossil Record, *Frontiers in Earth Science, 3,* 84. DOI: 10.3389/feart.2015.00084

Destainville, A., Champion, E., Bernache-Assollant, D., & Laborde, E. (2003). Synthesis, Characterization and Thermal Behavior of Apatitic Tricalcium Phosphate. *Materials Chemistry and Physics, 80,* 269-277. DOI: 10.1016/S0254-0584(02)00466-2

Eanes, E.D., Termine, J.D., & Nylen, M.U. (1973). An electron microscopic study of the formation of amorphous calcium phosphate and its transformation to crystalline apatite. *Calcified Tissue Research, 12,* 143–158. DOI: 10.1007/BF02013730

Eisa M.Y., Al Dabbas, M., & Abdulla, F.H. (2015). Quantitative identification of phosphate using X-ray diffraction and Fourier transform infrared (FTIR) spectroscopy. *International Journal of Current Microbiology and Applied Science, 4*(1), 270-283.

Elert, K., *Sánchez,* R.M.G., Benavides-Reyes, C., & Linares Ordóñez, F. (2019). Influence of animal glue on mineralogy, strength and weathering resistance of lime plasters. *Construction and Building Materials, 226*, 625-635. DOI: 10.1016/j.conbuildmat.2019.07.261

Franzoni, E., Graziani, G., Sassoni, E., Bacilieri, G., Griffa, M., & Lura, P. (2015). Solvent-based ethyl silicate for stone consolidation: influence of the application technique on penetration depth, efficacy and pore occlusion. *Materials and Structures, 48*, 3503-3515. DOI: 10.1617/s11527-014-0417-1

Fishman, M.R., Giglio, K., Fay, D. et al. (2018). Physiological and genetic characterization of calcium phosphate precipitation by *Pseudomonas* species. *Scientific Reports, 8,* 10156. DOI: 10.1038/s41598-018-28525-4

Gadd, G.M., Burford, E.P., & Fomina, M. (2003). Biogeochemical activities of microorganisms in mineral transformations: Consequences for metal and nutrient mobility. *Journal of Microbiology and Biotechnology, 13,* 323-331.

Han, J.K., Song, H-Y., Saito, F., & Lee, B-T. (2006). Synthesis of high purity nano-sized hydroxyapatite powder by microwave- hydrothermal method. *Materials Chemistry and Physics, 99*(2-3), 235-239. DOI: 10.1016/j.matchemphys.2005.10.017

Hammes, F., Boon, N., de Villiers, J., Verstraete, W., & Siciliano, S.D. (2003). Strain-specific ureolytic microbial calcium carbonate precipitation. *Applied and Environmental Microbiology*, *69*(8), 4901-4909. DOI: 10.1128/aem.69.8.4901-4909.2003

Jawaid, S., Ahmed, K., & Bhutto, M.A. (2018). Bio Concrete: An overview. *International Journal of Biology and Biotechnology, 15*(4), 801-813.

Kanth, A.P., & Singh, M.R. (2019). Spectroscopic and chromatographic investigation of the wall painted surface of an 18th century Falian Temple, New Delhi. *Vibrational spectroscopy, 104*, 102947. DOI: 10.1016/j.vibspec.2019.102947

Koutsopoulos, S. (2002). Synthesis and characterization of hydroxyapatite crystals: a review study on the analytical methods. *Journal of Biomedical Materials Research, 62*(4), 600-612.

Kumar, S., Vinodh., & Singh., M.R. (2019). Salt Weathering of 7th Century CE Granite Monument of Shore Temple, Mahabalipuram-Scientific Investigation and Conservation Strategy. *Heritage, 2*(1), 230-253. DOI: 10.3390/heritage2010017

Li, W., Chen, W.-S., Zhou, P.-P., Cao, L., & Yu, L.-J. (2012). Influence of initial pH on the precipitation and crystal morphology of calcium carbonate induced by microbial carbonic anhydrase. *Colloids and Surfaces B: Biointerfaces, 102,* 281–287. DOI: 10.1016/j.colsurfb.2012.08.042

Lowenstam, H.A., & Weiner, S. (1989). *On biomineralization*. Oxford University Press on demand. DOI: 10.1093/oso/9780195049770.001.0001

May, E. (2001). Novel approaches to conserve our european heritage: bioremediation for building restoration of the urban stone heritage in european states. *Biobrush research monograph: EVK4-CT,* 2001-00055, 2002-2005. https://cordis.europa.eu/project/id/EVK4-CT-2001-00055

Mobasherpour, I., Heshajin, M.S., Kozemzadeh, A., & Zakeri. M. (2007). Synthesis of nanocrystalline hydroxyapatite by using precipitation method. *Journal of Alloys and Compounds, 430,* 330-333.

Molina, L., Ramos., C., Duque, E., Ronchel, M.C., García., J.M., Wyke, L., & Ramos., J.L. (2000). Survival of *Pseudomonas putida* KT2440 in soil and in the rhizosphere of plants under greenhouse and environmental conditions. *Soil Biology and Biochemistry, 32*(3)*,* 315-321. DOI: 10.1016/S0038-0717(99)00156-X

Mpanga, I.K., Dapaah, H.K., Geistlinger, J., Ludewig, U., & Neumann, G. (2018). Soil Type-Dependent Interactions of P-Solubilizing Microorganisms with Organic and Inorganic Fertilizers Mediate Plant Growth Promotion in Tomato. *Agronomy, 8,* 213. DOI: doi.org/10.3390/agronomy8100213

Mpanga., I.K., Nkebiwe, P.M., Kuhlmann, M., Cozzolino, V., Piccolo, A., Geistlinger, J., Berger, N., Ludewig, U., & Neumann, G. (2019). The Form of N Supply Determines Plant Growth Promotion by P-Solubilizing Microorganisms in Maize. *Microorganisms*, *7*, 38. DOI: 10.3390/microorganisms7020038

Papayianni, I., & Stefanidou, M. (2001). The Evolution of Porosity in Lime Based Mortars. Proceedings of the 8th Euroseminar on Microscopy Applied to Building Materials, 4–7 September 2001, pp. 451-457, Athens, Greece.

Pedro, L.G., & de Brito, J. (2008). Quantifying environmental effects on cement rendered facades: A comparison between different degradation indicators. *Building and Environment, 43*(11), 1818-1828. DOI: doi.org/10.1016/j.buildenv.2007.10.022

Rainey, P.B. (1999). Adaptation of Pseudomonas fluorescens to the plant rhizosphere. *Environmental Microbiology, 1*(3), 243-257. DOI: 10.1046/j.1462-2920.1999.00040.x

Rajendran, C.P., Rajendran, K., Machado, T., Satyamurthy, T., Aravazhi, P., & Jaiswal M. (2006). Evidence of ancient sea surges at the mamallapuram coast of India and implications for previous Indian Ocean tsunami events. *Current Science, 91*(9), 1242-1247.

Ravi, R., Thirumalini, S., & Taher, N. (2018) Analysis of ancient lime plasters – Reason behind longevity of the Monument Charminar, India a study, *Journal of Building Engineering, 20*, 30-41. DOI: doi.org/10.1016/j.jobe.2018.04.010

Raynaud, S., Champion, E., Bernache-Assollant, D., & Thomas, P. (2002). Calcium phosphate apatites with variable Ca/P atomic ratio I. Synthesis, characterisation and thermal stability of powders. *Biomaterials*, *23*(4), 1065-1072. DOI: 10.1016/s0142-9612(01)00218-6

Rivadeneyra, M.A., Martín-Algarra, A., Sánchez-Román, M., Sánchez-Navas, A., & Martín-Ramos, J.D. (2010). Amorphous Ca-phosphate precursors for Ca-carbonate biominerals mediated by *Chromohalobacter marismortui*. *The ISME Journal, 4*(7), 922-932. DOI: 10.1038/ismej.2010.17

Nogueira, R., Pinto, A.P.F., & Gomes, A. (2018). Design and behavior of traditional lime-based plasters and renders. Review and critical appraisal of strengths and weaknesses. *Cement and Concrete Composites, 89*, 192-204. DOI: 10.1016/j.cemconcomp.2018.03.005

Rodriguez-Navarro, C., Rodriguez-Gallego, M., Chekroun, B.K., & Gonzalez-Muñoz, M.T. (2003). Conservation of ornamental stone by *Myxococcus xanthus*-induced carbonate biomineralization. *Applied and Environmental Microbiology, 69*(4), 2182-2193. DOI: 10.1128/aem.69.4.2182-2193.2003

Sathyabhama, B., Hema, A., Smriti, H., & Mohandas, K.P. (2011). Salvankuppam Coastal temple, excavation and application of soil micromorphology. *Current Science, 100*(7), 1071-1075.

Sickels, L.-B. (1982). Organics vs. synthetics: Their use as additives in mortars. Mortars, Cement and Grouts used in the Conservation of Historical Buildings Symposium, 3–6 November 1981, Rome: Iccrom.

Singh, M.R., & Vinodh Kumar, S. (2019). Architechtural features and characterization of 16th century Indian Monument Farah Bagh, Ahmed Nagar, India. *International Journal of Architectural Heritage, 14*(9), 1398-1411. DOI: 10.1080/15583058.2019.1610524

Sigel, A., Sigel, H., & Sigel, R.K.O. (2008) *Biomineralization: From nature to application, Volume 4.* Metal Ions in Life Sciences, John Wiley & Sons.

Sundaresh, A.S. Gaur, Tripathi, S., & Vora, K.H. (2004). Underwater investigations of Mahabalipuram, Tamil Nadu. *Current Science, 86*(9), 1231-1237.

Tao, J. (2013). Chapter Twenty-Two - FTIR and Raman Studies of Structure and Bonding in Mineral and Organic–Mineral Composites. *Methods in Enzymology, 532*, 533-556. DOI: 10.1016/B978-0-12-416617-2.00022-9

Turner, R.J., Renshaw, J.C., & Hamilton. A. (2017). Biogenic Hydroxyapatite: A New Material for the Preservation and Restoration of the Built Environment. *ACS Applied Materials & Interfaces, 9*(37), 31401-31410. DOI: 10.1021/acsami.7b07927

Zhao, P., Jackson, M.D., Zhang, Y., Li, G., Monteiro, P.J.M., & Yang, L. (2015). Material characteristics of ancient Chinese lime binder and experimental reproductions with organic admixtures. *Construction and Building Materials, 84*, 477-488. DOI: doi.org/10.1016/j.conbuildmat.2015.03.065

Received: 3 August 2021
Accepted: 30 January 2022
Handling Editor: Tomasz Bajda